Sensitivity of the Helium and Lead Observatory to Core-Collapse Supernova Neutrino Bursts

Thesis by

John Franklin Crenshaw

Honors Thesis submitted in partial fulfillment of the requirements for
Graduation with Distinction with the degree of Bachelor of Science

Department of Physics

Duke University

2019

Committee Members:

Prof. Kate Scholberg, Advisor

Prof. Chris Walter

Prof. Joshua Socolar

Abstract

Core-collapse supernovae release 99% of their energy via neutrino emission. These neutrinos stream out of the dying star, carrying with them unique information about supernova and neutrino dynamics, as well as providing advance warning to astronomers of the supernova's optical signal. The Helium and Lead Observatory (HALO) is a detector at SNOLAB waiting to detect these supernova neutrino bursts via charged- and neutral-current interactions with the detector's lead nuclei. Depending on neutrino energies, interactions with lead may produce neutrons, either singly (1n) or in pairs (2n). The number of 1n and 2n events is sensitive to the neutrino spectrum. It is therefore important to evaluate HALO's detection efficiency and to develop a method for reconstructing true 1n and 2n numbers from detected events. A full Geant4 simulation of the detector is used to determine HALO's detection efficiencies. These efficiencies are used in Monte Carlo studies to improve the unfolding process, which previously resulted in large uncertainties and unphysical predictions. These problems are alleviated by a Bayesian algorithm, but this raises the question of how to select a prior. Three different priors are constructed with reference to expected event numbers as calculated with the SNOwGLoBES event rate calculator. This analysis also allows the development of a figure of merit which quantifies HALO's sensitivity versus supernova distance. It is found that the sensitivity of HALO is roughly limited to 5 kpc, with weak sensitivity in the 5-10 kpc range. Similar studies are performed for HALO-1kT, the proposed 1 kiloton upgrade at Gran Sasso National Laboratory (LNGS) in Italy. HALO-1kT has much smaller unfolding uncertainties, and is sensitive to supernovae 5 times farther than HALO.

To my Father, whose curiosity
and passion set me on this path.
I love and miss him dearly.

Contents

List of Figures

Acknowledgements

I would like to thank Prof. Kate Scholberg for her mentorship and the countless opportunities she has made available to me over the last three years. I would also like to thank Prof. Chris Walter, Gleb Sinev, Justin Raybern, and Erin Conley for their help and support, and the rest of the Neutrino and Cosmology Group for their friendship. In addition, I would like to thank Prof. Barry Pointon for providing me with the Garching, GVKM, and Basel-Darmstadt event numbers, and the rest of the HALO Collaboration for their advice.

This research was funded by the National Science Foundation.

1

Neutrino Physics

In the Standard Model of particle physics, particles are divided into two groups: the bosons, with integer spin, and the fermions, with half-integer spin. The fermions are further divided into the quarks, which experience the strong nuclear force, and the leptons, which do not (Figure 1.1). The uncharged leptons are known as the neutrinos.

Neutrinos are elusive particles, as they do not interact via the strong or electromagnetic forces, and have extremely small masses (less than a millionth the mass of the electron). As a result, neutrinos can travel through light minutes of lead without interacting at all. The extreme rarity of neutrino interactions makes the particles both very difficult to detect and also very useful scientific probes (in addition to being incredibly interesting in their own right). Using neutrinos as probes of supernova dynamics will be discussed in Chapter 2.

There are six neutrinos: three "flavors" and their corresponding anti-particles. The three flavors, electron, muon, and tau (ν_e, ν_μ, ν_τ respectively) are named and identified by the charged lepton they are associated with via weak interactions. For example, the electron anti-neutrino is always produced with the electron in beta decay ($n \rightarrow p + e^- + \bar{\nu}_e$). Some experimental anomalies and theoretical arguments have led to proposals of additional, "sterile" neutrino flavors that do not interact via the weak force [2]. Sterile neutrinos remain hypothetical and will not be considered here.

Perhaps the most fascinating property of neutrinos is their mass, which was initially assumed to be zero. While the neutrino masses have not yet been directly measured, they have been indirectly probed via neutrino flavor oscillation.

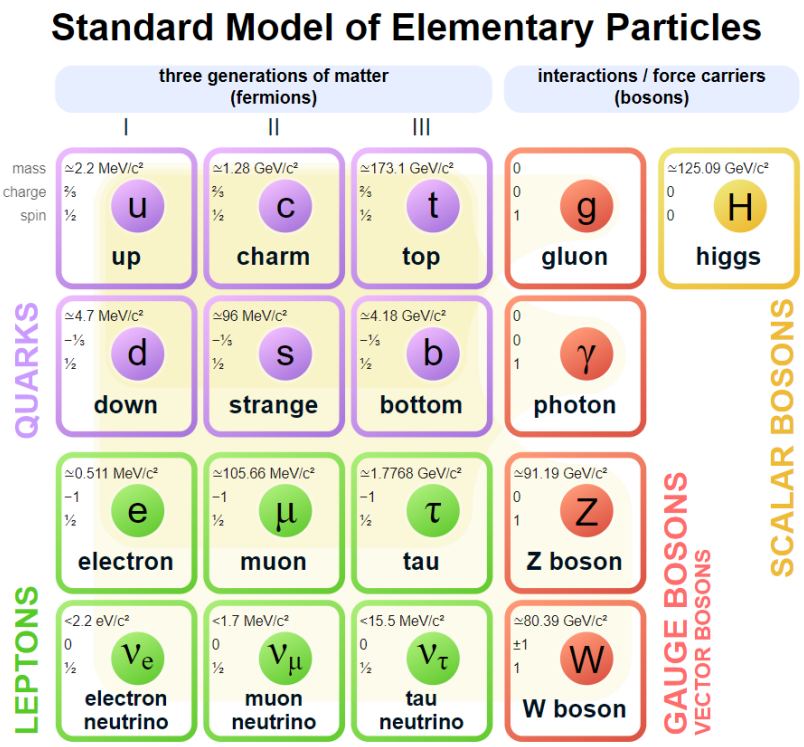

Figure 1.1: The particles of the Standard Model. Figure from [1].

1.1 Neutrino Flavor Oscillations

Unlike the charged leptons, the neutrino flavor eigenstates are not mass eigenstates. Each neutrino flavor $(\nu_e, \nu_\mu, \nu_\tau)$ is a linear combination of the three mass states (ν_1, ν_2, ν_3). This can be expressed

$$|\nu_\ell\rangle = \sum_{i=1}^{3} U^*_{\ell i} |\nu_i\rangle \quad \text{with} \quad \begin{cases} \ell = e, \mu, \tau & \text{[flavor]} \\ i = 1, 2, 3 & \text{[mass]} \end{cases}, \tag{1.1}$$

where $U^*_{\ell i}$ are components of the complex conjugate of the Pontecorvo-Maki-Nakagawa–Sakata (PMNS) matrix, whose entries depend on the leptonic mixing angles $(\theta_{13}, \theta_{12}, \theta_{23})$ and the CP violating phase δ [3]. This superposition gives rise to the flavor oscillation that serves as indirect evidence of a non-zero neutrino mass. Let us investigate.

All particles propagate according to the Schrödinger equation

$$i\hbar\frac{\partial}{\partial t}\left|\psi(t)\right\rangle = \hat{H}\left|\psi(t)\right\rangle. \tag{1.2}$$

Using natural units, the solution for a neutrino mass eigenstate j is

$$\left|\nu_j(t)\right\rangle = e^{-iE_j t}\left|\nu_j(0)\right\rangle. \tag{1.3}$$

Combining Equations 1.1 and 1.3, we can describe the propagation of a neutrino of flavor α:

$$\begin{aligned}
\left|\nu_\alpha(t)\right\rangle &= \sum_j U^*_{\alpha j}\left|\nu_j(t)\right\rangle \\
&= \sum_j U^*_{\alpha j} e^{-iE_j t}\left|\nu_j(0)\right\rangle \\
&= \sum_j U^*_{\alpha j} e^{-iE_j t}\left(\sum_\ell U_{\ell j}\left|\nu_\ell(0)\right\rangle\right) \\
&= \sum_\ell \left(\sum_j U^*_{\alpha j} e^{-iE_j t} U_{\ell j}\right)\left|\nu_\ell(0)\right\rangle.
\end{aligned} \tag{1.4}$$

The transition amplitude is then

$$\left\langle\nu_\beta|\nu_\alpha(t)\right\rangle = \sum_j U^*_{\alpha j} U_{\beta j} e^{-iE_j t}, \tag{1.5}$$

giving a transition probability of

$$\begin{aligned}
P(\nu_\alpha \to \nu_\beta) &= \left|\left\langle\nu_\beta|\nu_\alpha(t)\right\rangle\right|^2 \\
&= \sum_{j,k} U^*_{\alpha j} U_{\beta j} U_{\alpha k} U^*_{\beta k} e^{-i(E_j - E_k)t} \\
&= \sum_j \left|U_{\alpha j}\right|^2 \left|U_{\beta j}\right|^2 + 2\sum_{j>k} \mathrm{Re}(Q^*_{\alpha\beta,\,jk})\cos(\Delta E_{jk}\ t) \\
&\qquad + 2\sum_{j>k} \mathrm{Im}(Q^*_{\alpha\beta,\,jk})\sin(\Delta E_{jk}\ t)
\end{aligned}$$

$$
\begin{aligned}
&= \sum_j |U_{\alpha j}|^2 \, |U_{\beta j}|^2 + 2 \sum_{j>k} \mathrm{Re}(Q^*_{\alpha\beta,\,jk}) \\
&\quad - 4 \sum_{j>k} \mathrm{Re}(Q^*_{\alpha\beta,\,jk}) \sin^2 \left(\frac{\Delta E_{jk}}{2} \, t \right) + 2 \sum_{j>k} \mathrm{Im}(Q^*_{\alpha\beta,\,jk}) \sin(\Delta E_{jk} \, t) \\
&= \delta_{\alpha\beta} - 4 \sum_{j>k} \mathrm{Re}(Q^*_{\alpha\beta,\,jk}) \sin^2 \left(\frac{\Delta E_{jk}}{2} \, t \right) + 2 \sum_{j>k} \mathrm{Im}(Q^*_{\alpha\beta,\,jk}) \sin(\Delta E_{jk} \, t), \quad (1.6)
\end{aligned}
$$

where in line 3 I used the quartet $Q_{\alpha\beta,\,jk} = U_{\alpha j} U^*_{\beta j} U^*_{\alpha k} U_{\beta k}$, and $\Delta E_{jk} = E_j - E_k$, and in line 5 I used

$$
P(t=0) = \sum_j |U_{\alpha j}|^2 \, |U_{\beta j}|^2 + 2 \sum_{j>k} \mathrm{Re}(Q^*_{\alpha\beta,\,jk}) = \delta_{\alpha\beta}. \quad (1.7)
$$

Assuming that the neutrino is relativistic, which is reasonable considering the their tiny mass, $t \approx L$ and $E = \sqrt{p^2 + m^2} \approx p + \frac{m^2}{2E}$. Equation 1.6 is then

$$
\begin{aligned}
P(\nu_\alpha \to \nu_\beta) = \delta_{\alpha\beta} &- 4 \sum_{j>k} \mathrm{Re}(Q^*_{\alpha\beta,\,jk}) \sin^2 \left(\frac{\Delta m^2_{jk}}{4E} L \right) \\
&+ 2 \sum_{j>k} \mathrm{Im}(Q^*_{\alpha\beta,\,jk}) \sin \left(\frac{\Delta m^2_{jk}}{2E} L \right), \quad (1.8)
\end{aligned}
$$

where $\Delta m^2_{jk} = m^2_j - m^2_k$.

It can be seen from Equation 1.8 that the probability of a neutrino of flavor α being detected as flavor β oscillates as the neutrino propagates through space. This is what is meant by "flavor oscillation". This oscillation is depicted as a function of propagation distance L in Figure 1.2.

There are several important features of neutrino oscillations to note. Firstly, if the parameter Δm^2_{jk} is zero, oscillations do not occur. Thus, neutrino oscillations indicate that the neutrinos have non-degenerate masses. The detection of oscillation in solar neutrinos provided the first evidence for non-zero neutrino mass, for which Takaaki Kajita and Arthur McDonald were awarded the Nobel Prize in Physics in 2015. Note, however, that neutrino oscillations are only sensitive to the differences of the squared masses and not to the abso-

lute mass scale. The absolute neutrino masses are not currently known but observations in cosmology have imposed an upper limit of 0.3 eV on their sum [4]. Furthermore, over the course of the next few years, the KATRIN experiment is expected to measure the absolute masses (or further lower the upper limit) from the decay spectrum of tritium.

In addition to the absolute mass scale, we do not know the neutrino "mass hierarchy". It is impossible to tell from Δm^2_{21} and Δm^2_{31} alone whether ν_3 is heavier (normal hierarchy, NMH) or lighter (inverted hierarchy, IMH) than ν_1 and ν_2. While the true hierarchy is currently unknown, recent experiments favor the NMH [5, 6].

In addition to the vacuum oscillations described here, there are further oscillation contributions when neutrinos travel through matter. The Mikheyev–Smirnov–Wolfenstein (MSW) effect accounts for the forward scattering of electron neutrinos and anti-neutrinos off electrons in matter, which can increase the flavor mixing (See Section 2.2). In addition, there are "collective" effects when neutrinos propagate through regions of extremely high neutrino

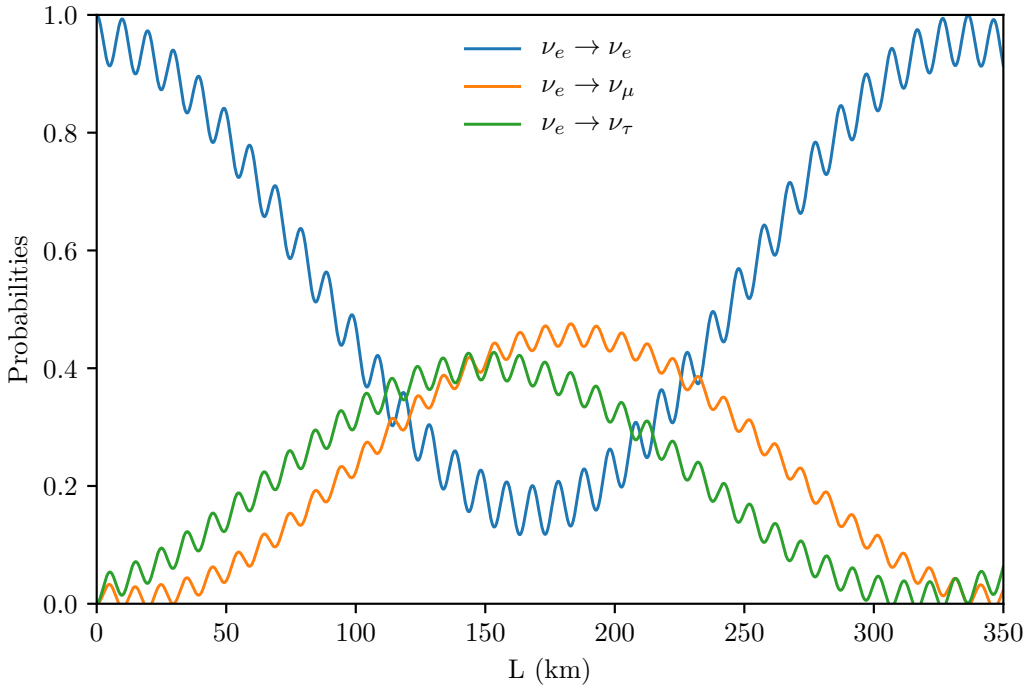

Figure 1.2: Flavor oscillation of a 10 MeV electron neutrino as it propogates through 350 km. Calculated using Equation 1.8 and oscillation parameters from the Particle Data Group.

density (e.g. in core-collapse supernovae), which result in a swap in the energy spectra of ν_e and ν_μ, ν_τ [3].

Finally, as mentioned above, the parameterization of the PMNS matrix involves a CP-violating phase δ. If δ is non-zero, then $P(\nu_\alpha \rightarrow \nu_\beta) \neq P(\bar{\nu}_\alpha \rightarrow \bar{\nu}_\beta)$, indicating that neutrino oscillations violate CP symmetry. This violation could provide a solution to the baryon asymmetry problem [7].

2

Supernova Neutrinos

2.1 Core-Collapse Supernovae

For most of their million and billion year life cycles, stars fuse hydrogen in their cores, creating Helium nuclei and the pressure necessary to sustain themselves against the pull of gravity. When the hydrogen in the core is depleted, the core contracts and fusion of helium begins, generating carbon and oxygen. Fusion of hydrogen also resumes in a shell surrounding the core, causing the star to expand and cool, becoming a red giant. This is as far as most stars evolve, as they are not sufficiently massive to fuse heavier elements. This final configuration is unstable, and via a series of pulses, the star ejects approximately half of its mass, leaving a white dwarf star surrounded by a planetary nebula [8].

Stars more massive than 8 $M_\odot$ are able to proceed past carbon and oxygen. These stars continue to produce heavier and heavier elements in their core, until they reach iron. As iron has the greatest binding energy, creation of heavier elements is no longer exothermic and will not support the star. The final stage of these stars is like an onion, with an inert iron core, surrounded by shells of progressively lighter elements, at lower densities and temperatures. The iron core, no longer undergoing fusion, is supported merely by electron degeneracy pressure. When the mass of the star's core reaches the Chandrasekhar limit of 1.4 $M_\odot$, electron degeneracy pressure can no longer prevent gravitational collapse [9]. This begins the supernova[1], a massive explosion which rips the star apart.

In a fraction of a second, the core implodes from approximately the size of the Earth to

[1]Supernovae can also occur when a white dwarf star surpasses the Chandrasekhar limit by siphoning mass from its binary partner. These supernovae (type Ia) are famously important as standard candles, but they do not produce significant neutrino signals [10]. Unless otherwise stated, all mentions of supernovae in this thesis refer to core-collapse supernovae.

the size of a city, achieving densities greater than an atomic nucleus [9]. When the core of the star can no longer contract, the infalling matter rebounds, "bouncing" off the core and slamming into the surrounding mantle. This collision stalls the explosion. However, during the supernova, a prodigious number of neutrinos are created, which scatter off the matter in the super-dense core. A massive shock wave is driven outward, ripping apart the star and launching heavy elements into the cosmos. These cataclysmic explosions often outshine their own host galaxies for several days [9]. Depending on the mass of the progenitor, either a neutron star or a black hole is left as a remnant.

2.2 Neutrinos from Core-Collapse

Supernovae are extremely energetic events that can outshine their host galaxy; however only 0.01% of the progenitor's gravitational binding energy is released in photons. Approximately 1% of the energy is in the kinetic energy of the ejecta, but 99% of the energy is radiated as neutrinos.

The supernova process begins when the gravitational pull of the inert iron core exceeds the electron degeneracy pressure. Electrons in the core begin to combine with protons in a process known as neutronization ($p + e^- \rightarrow n + \nu_e$). Neutronization reduces the volume of the core, allowing it to collapse under the force of gravity, and releases a large number of electron neutrinos. These neutrinos are trapped for tens of milliseconds by the extreme density of matter in the core, afterwhich they stream out of the star. This is visible in supernova neutrino fluxes as an early spike of electron neutrinos, during which the ν_e luminosity is of the order 10^{53} erg s^{-1} (0.06 $M_\odot c^2$ per second).

The next phase of the supernova, the stall of the shock wave and subsequent neutrino heating, lasts around a second. Features of the neutrino signal during this stage of the explosion are likely to yield valuable information about supernovae and the formation of supernova remnants. During this phase, the star begins to produce muon and tau neutrinos via thermal processes: via pair production ($e^+ + e^- \rightarrow \nu + \bar{\nu}$), photo-annihilation ($e^- + \gamma \rightarrow e^- + \nu + \bar{\nu}$), plasmon decay ($\gamma^* \rightarrow \nu + \bar{\nu}$), and nucleon-nucleon bremsstrahlung ($e^- + (Z, A) \rightarrow$

$(Z, A) + e^- + \nu + \bar{\nu})$ [10]. We consider ν_μ, ν_τ, and their anti-particles together as ν_x as they are produced and interact almost identically in the supernova, and are essentially impossible to distinguish observationally.

In the final stage of the supernova, all three neutrino flavors and their anti-particles are produced in large, roughly equal luminosities. This stage lasts tens of seconds, during which neutrinos stream freely out of the supernova, gradually decreasing in luminosity and energy.

Although all neutrino flavors have approximately equal luminosities, the details of their spectra vary, depending on their interactions with matter in the proto-neutron star. The ν_e interact with the matter the most, and thus decouple later and tend to be cooler. The $\bar{\nu}_e$ interact less, as there are fewer protons than neutrons, so their charged-current interactions are suppressed. As a result, they decouple deeper in the proto-neutron star and tend to be hotter. The ν_x are the hottest, as they have only neutral-current interactions, and thus decouple earliest. These different decoupling depths establish a hierarchy of average energies $\langle E_{\nu_e} \rangle < \langle E_{\bar{\nu}_e} \rangle < \langle E_{\nu_x} \rangle$ [10].

There will be other signatures in the neutrino flux as a result of neutrino flavor oscillations. Oscillations are affected by the density of the matter and the propagation of the shock wave. The neutrino density in a supernova is so great that "collective effects," i.e. neutrino-neutrino interactions, become relevant. This complex, non-linear phenomenon swaps the energy spectra of different flavors. The process is not yet fully understood, and data from supernova neutrinos would be invaluable. In addition, the ν_e from the neutronization burst are free from collective effects, and thus would only be affected by the MSW effect. We expect that the ν_e flux at Earth would be

$$F_{\nu_e} = F^0_{\nu_x} \qquad \text{(NMH)} \tag{2.1}$$

$$F_{\nu_e} = \sin^2\theta_{12} F^0_{\nu_e} + \cos^2\theta_{12} F^0_{\nu_x} \qquad \text{(IMH)}, \tag{2.2}$$

thus suppression of the neutronization burst would be strong evidence of the NMH [11].

There has been one detection of a supernova neutrino burst. In 1987, neutrinos from a

supernova in the Large Magellanic Cloud were observed in several detectors on Earth. The neutrinos from this supernova, 1987A, confirmed our basic ideas about supernova neutrino bursts, but not enough were detected to discriminate between different supernova models [12]. We will be ready to learn much more from the next galactic supernova, and we are prepared to coordinate neutrino detections to forewarn astronomers of the optical signal (See Section 2.3).

In summary, neutrinos are produced in extreme quantities during a core-collapse supernova. The weakness of neutrino interactions allow them to carry valuable information about supernova dynamics out of the star. By detecting these fluxes, we can learn about supernova mechanisms and remnant formation. In addition, we can learn more about neutrinos themselves, such as the hierarchy of their masses and how they interact with each other.

2.3 The SuperNova Early Warning System (SNEWS)

Since neutrinos decouple from the supernova on the order of seconds, compared to the hours it takes for the photons to decouple, the neutrino flux should arrive at Earth prior to the optical signal. The SuperNova Early Warning System (SNEWS) plans to take advantage of this time delay to forewarn astronomers of a galactic supernova so that the optical signal can be viewed from the beginning. SNEWS is an international network that currently consists of 7 neutrino detectors: Super-K (Japan), LVD (Italy), Ice Cube (South Pole), KamLAND (Japan), Borexino (Italy), Daya Bay (China), and HALO (Canada). These experiments report neutrino bursts to a central system that will send out an alert to scientists if multiple experiments detect a burst simultaneously. It is hoped that we will be able to use data from several experiments together to quickly triangulate the location of the impending supernova. There are many checks in place to avoid a false-positive. More information can be found in Reference [13].

3

The Helium and Lead Observatory

3.1 The HALO Detector

The Helium and Lead Observatory (HALO) is a supernova neutrino detector at SNOLAB in Ontario, Canada. The detector consists of a 79-ton lead matrix, instrumented with 128 ^{3}He counters (Figure 3.1). During a supernova neutrino burst, neutrinos will interact with the lead nuclei, causing them to emit neutrons that are detected by the ^{3}He counters.

HALO was built to be a low-cost, low-maintenance detector. The lead ingots were recycled from the decommissioned Canadian Deep River cosmic ray station. The ^{3}He counters and associated electronics were recycled from the SNO experiment. Furthermore, since the goal of HALO is to detect galactic supernovae, which occur about once every thirty years, the detector is designed to run for long periods with minimal downtime and maintenance. The detector has many redundant systems, such as two DAQ computers, a backup power supply [14].

The HALO lead matrix is 206 cm tall, 243 cm wide, and 308 cm deep. The matrix is supported by a steel structure and iron rings to prevent sagging. The lead is surrounded by boxes of water and plastic boards for neutron shielding. The matrix contains 32 bores, each housing four ^{3}He neutron counters. Each counter is 5 cm in diameter and 2.5 to 3 meters long. Each contains an 85:15 mixture of ^{3}He and and CH_4 at a pressure of 2.5 atm [14]. The counters are proportional counters, meaning the voltage they produce is proportional to the energy deposition in the gas. The entire detector is constructed from low-background materials.

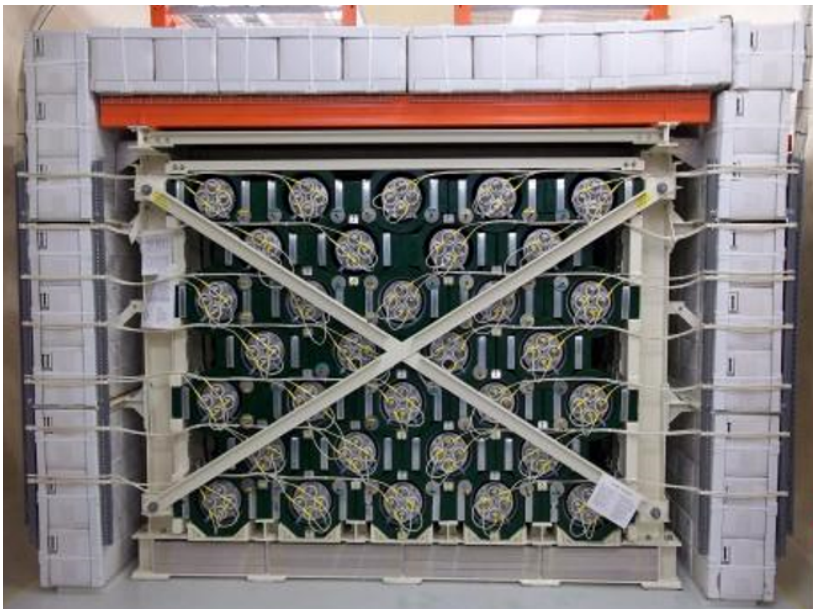

Figure 3.1: The HALO detector, with the front face open. The lead matrix is painted dark green, while the steel supports are white. The detector sits on plastic lumber and is surrounded by boxes of water for neutron blocking.

3.2 Neutrino Detection in Lead

In the event of a galactic supernova, many experiments around the world will observe a neutrino burst, but HALO is the only experiment that will detect neutrinos with lead. Most detectors are primarily sensitive to electron anti-neutrinos via inverse beta decay, $\bar{\nu_e} + p \rightarrow n + e^+$, but have little sensitivity to the other flavors. However, this interaction is Pauli blocked in lead, which is neutron rich. As a result, lead detectors like HALO are sensitive to ν_e through charged-current (CC) interactions, and ν_x and $\bar{\nu}_x$ via neutral-current (NC) interactions.

The most important interactions in HALO are

$$\nu_e + {}^{208}\mathrm{Pb} \rightarrow {}^{207}\mathrm{Bi} + n + e^- \tag{3.1}$$

$$\nu_e + {}^{208}\mathrm{Pb} \rightarrow {}^{206}\mathrm{Bi} + 2n + e^- \tag{3.2}$$

$$\nu_x + {}^{208}\mathrm{Pb} \rightarrow {}^{207}\mathrm{Pb} + n \tag{3.3}$$

$$\nu_x + {}^{208}\mathrm{Pb} \rightarrow {}^{206}\mathrm{Pb} + 2n \tag{3.4}$$

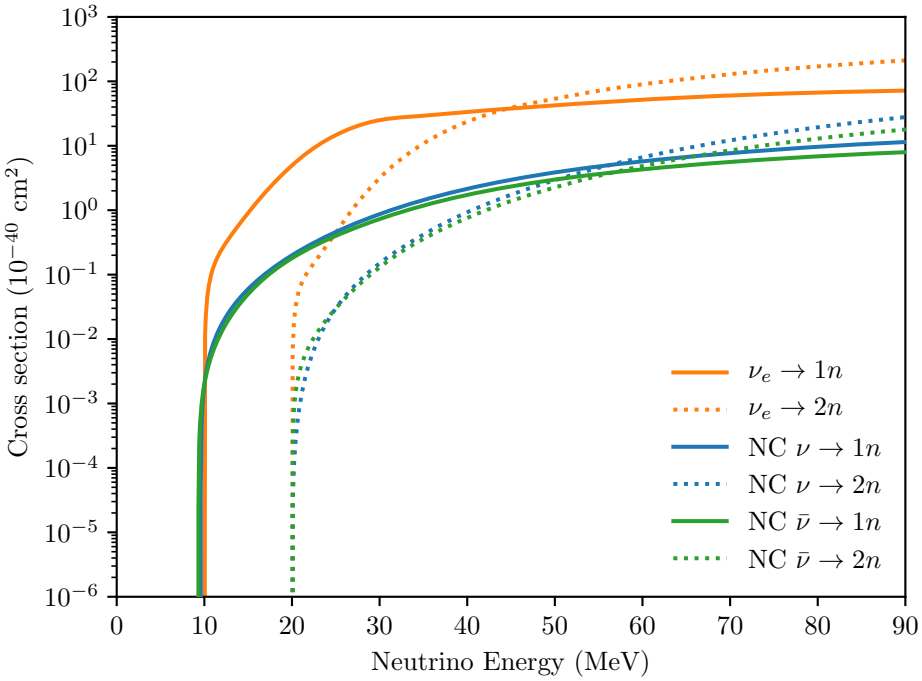

Figure 3.2: Cross sections for 1n and 2n production in lead. 2n production cuts off sharply around 20 MeV. Data from [16].

In reality, only half of natural lead is ^{208}Pb, but the cross sections for the other isotopes will be nearly identical [15]. Whether the neutrino interaction produces a single (1n) or double (2n) neutron event depends on the energy of the incident neutrino (3n+ events are also possible but are negligible for the relevant energies). Supernova neutrinos will have energies in the tens of MeV, and it can be seen in Figure 3.2 that 2n events cut off sharply at neutrino energies around 20 MeV. Thus the ratio of 1n to 2n events is sensitive to the neutrino spectra, which contain important information about supernova dynamics and neutrino properties (see Chapter 2).

Ejected neutrons scatter off lead nuclei unabsorbed, as the lead nuclei are already neutron rich, so their neutron capture cross sections are low. The lead nuclei moderate fast neutrons until they thermalize. Many of these thermalized neutrons enter one of the ^{3}He counters embedded throughout the matrix. ^{3}He has a cross section of 5334 barns for thermal neutron capture [14]. As a result, on entering a ^{3}He counter, the neutron is captured by ^{3}He to create an excited state of ^{4}He, which then decays: $^4\text{He}^* \to ^3\text{H} + p + 764$ keV. The triton and proton

ionize the gas, and the free electrons are collected on a 1.7 kV anode wire running down the center of the counter [14].

Many of the neutrino-induced-neutrons will escape HALO undetected. In order to properly calculate the ratio of 1n to 2n events, the observed data must be "unfolded" to infer the true number of 1n and 2n events. In order to perform this unfolding, we must run simulations to understand the efficiencies of the HALO detector (See Chapter 4).

3.3 HALO-1kT

The small mass of HALO means that in the event of a galactic supernova, HALO will have relatively low statistics (see Section 4.1). In addition, HALO's low mass means that HALO has poor sensitivity to supernovae much further than 5 kpc (see Chapter 6). This is problematic, as the most likely distance to a galactic supernova is approximately 10 kpc [10]. HALO's shortcomings, combined with the high science potential of a lead-based neutrino detector, motivates a mass upgrade for HALO. The currently envisioned upgrade, HALO-1kT, would consist of a kiloton of lead.

The decommissioning of the OPERA neutrino experiment at LNGS has made over 1000 tons of low activity lead available, providing an opportunity for a relatively low-cost HALO upgrade. The design of HALO-1kT has already been under development for some time. Cheaper construction of ^{3}He tubes is being investigated and Monte Carlo simulations are being performed to optimize the configuration of the new detector. The current concept is for a 4.3 x 4.3 x 5.5 meter matrix of lead, instrumented with a 28x28 grid of ^{3}He counters [17].

In the following, preliminary analysis for this configuration of HALO-1kT will be performed alongside the HALO analysis. This will allow us motivate and evaluate the merit of a 1 kiloton HALO upgrade.

4

Simulating Neutrino Detection in HALO

In order to perform data unfolding studies for HALO, it is necessary to simulate the detection process. This conists of two stages. First, we must determine the expected range of 1n and 2n events that will occur in HALO for a typical supernova. This is the topic of Section 4.1. Second, we must simulate the detection of these truth events in the detector. This is the subject of Section 4.2.

4.1 Expected Event Numbers in HALO

Supernova neutrino fluxes can be approximated by a Fermi-Dirac distribution. However, as supernova neutrinos are not thermal, this approximation is a poor fit for the high energy tail, which can have a large impact on the number of neutrino detections. Instead, we use the quasiempirical parameterization:

$$\phi(E_\nu) = N_0 \frac{(\alpha+1)^{\alpha+1}}{\langle E_\nu \rangle \Gamma(\alpha+1)} \left(\frac{E_\nu}{\langle E_\nu \rangle} \right)^\alpha \exp\left[-(\alpha+1) \frac{E_\nu}{\langle E_\nu \rangle} \right], \tag{4.1}$$

where E_ν is the neutrino energy, $\langle E_\nu \rangle$ is the mean neutrino energy, α is a "pinching parameter," Γ is the gamma function, and N_0 is the total number of neutrinos [18]. This is a Fermi-Dirac-like distribution, where α controls the suppression of the high-energy tail: larger α means a more suppressed tail, whereas $\alpha < 1$ indicates an enhanced tail. The pinching parameter can have a large effect on event rates, as neutrino cross sections often scale quadratically with energy [10]. This spectrum is fully described by three parameters — $L,\ \langle E_\nu \rangle,\ \alpha$ — where $L = N_0 \cdot \langle E_\nu \rangle$ is the total luminosity. Figure 4.1 shows the fluxes of $\nu_e,\ \bar{\nu}_e,\ \nu_x$ for a specific choice of parameters, while Figure 4.2 shows the ν_x flux for a variety

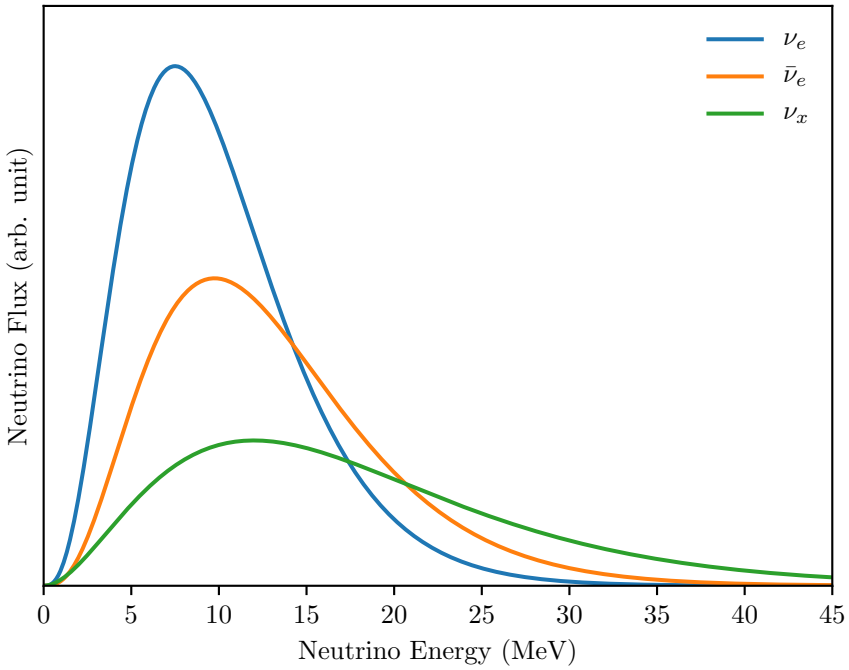

Figure 4.1: Neutrino spectra at the neutrinosphere for a specific choice of parameters in Equation 4.1: $L_{\nu_e} = L_{\bar{\nu}_e} = L_{\nu_x}$, $\langle E_{\nu_e} \rangle = 10$ MeV, $\langle E_{\bar{\nu}_e} \rangle = 13$ MeV, $\langle E_{\nu_x} \rangle = 18$ MeV, $\alpha_{\nu_e,\bar{\nu}_e} = 3$, and $\alpha_{\nu_x} = 2$.

of different ν_x parameters.

The expected number of 1n and 2n events in HALO is calculated for a variety of ν_x parameters in Equation 4.1. Following the work by Väänänen and Volpe [19], I set $L_{\text{tot}} = 10^{52}$ erg/s, for a duration of 10 s. I fix $\langle E_{\nu_e} \rangle = 10$ MeV, $\langle E_{\bar{\nu}_e} \rangle = 13$ MeV, and $\alpha_{\nu_e,\bar{\nu}_e} = 3$. I then consider L_{ν_x} with equipartition ($L_{\nu_x} = L_{\nu_e} = L_{\bar{\nu}_e}$) and an extreme case of $L_{\nu_x} = 2L_{\nu_e,\bar{\nu}_e}$. I considered $\langle E_{\nu_x} \rangle = 15$, 18, 25 MeV, and let α_{ν_x} vary from 2 to 7. With these fluxes, the number of 1n and 2n events in HALO is predicted using the SNOwGLoBES event rate calculator [20]. SNOwGLoBES also includes flavor oscillations, which are performed twice: once assuming NMH, and once assuming IMH. These predictions can be seen as the red and blue curves in Figure 4.3. SNOwGLoBES does not currently include collective effects in the oscillations, which may be substantial. These effects must be taken into account for a more complete analysis.

In addition to the fluxes modeled by Equation 4.1, a variety of other specific flux mod-

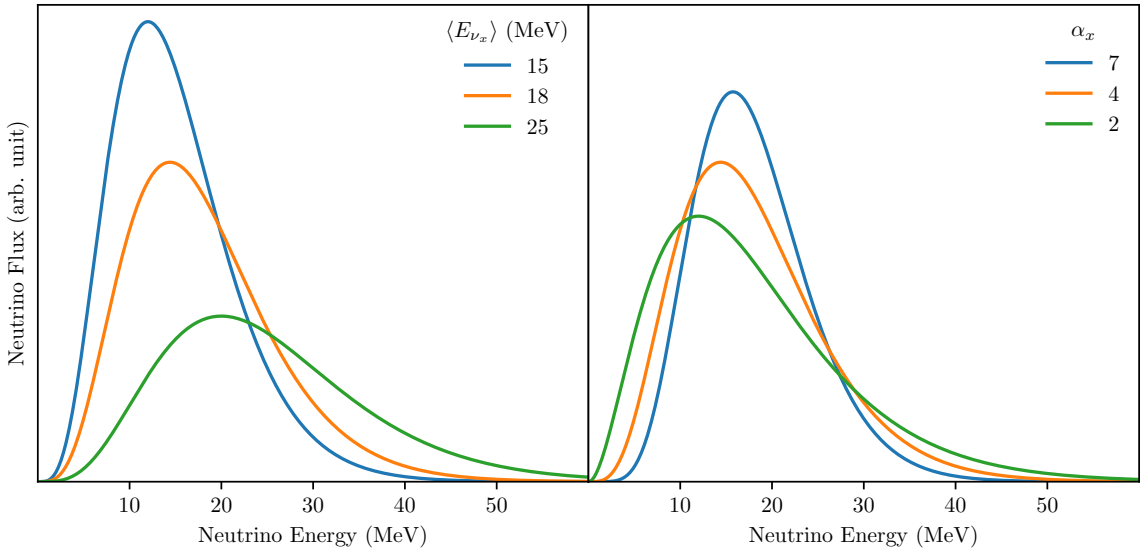

Figure 4.2: Spectra of ν_x for a variety of parameters in Equation 4.1. Left: varying $\langle E_{\nu_x} \rangle$ while $\alpha_{\nu_x} = 4$. Right: varying α_{ν_x} while $\langle E_{\nu_x} \rangle = 18$ MeV.

els from the literature are considered. The expected event numbers for these models were calculated with SNOwGLoBES and plotted in Figure 4.3. The blue "Garching" fluxes are from Hüdepohl et al. [21], the pink "GVKM" fluxes from Gava et al. [22], and the green "Basel-Darmstadt" fluxes from Bandyopadhyay et al. [23]. The black "LS220" and gray "Shen" squares represent fluxes from the PhD thesis of L. Hüdepohl [24]. The specifics of these supernova neutrino models will not be discussed here, but the expected number of events in HALO for these models can be found in the appendix.

Event numbers in HALO can be easily calculated for supernovae at different distances by scaling as $1/r^2$. In addition, event numbers for HALO-1kT can be calculated from the HALO numbers simply via scaling by the mass ratio (1/0.079). Event numbers in HALO-1kT for a supernova at 10 kpc can be found in Figure 4.4.

4.2 Neutron Detection Efficiency

Given the expected range of 1n, 2n events in HALO for a variety of supernova neutrino flux models, we need to determine how efficient HALO is at detecting these events.

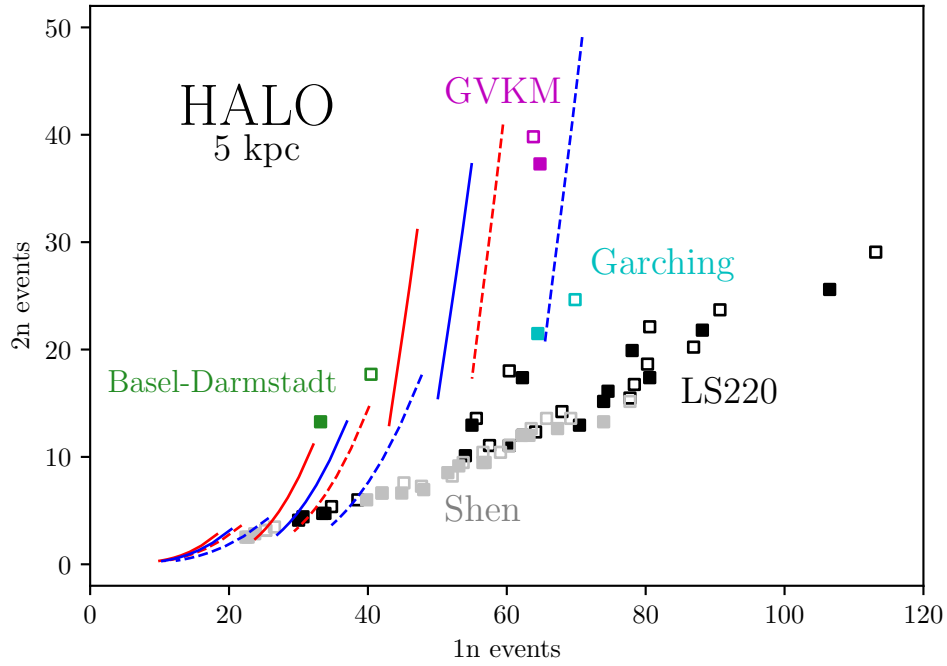

Figure 4.3: Expected number of 1n and 2n events in HALO for various neutrino flux models for a supernova at 5 kpc. Red and blue curves represent various ν_x parameters for Equation 4.1. Red: $L_{\nu_x} = L_{\nu_e,\bar{\nu}_e}$; Blue: $L_{\nu_x} = 2L_{\nu_e,\bar{\nu}_e}$. α_{ν_x} varies from 2 at the top of the curves to 7 at the bottom. Dashed curves were oscillated assuming NMH; solid curves IMH. The three sets of each curve represent, from left to right, $\langle E_{\nu_x} \rangle = 15$, 18, 25 MeV. The squares are fluxes from References [21, 22, 23, 24]. Open squares were oscillated assuming NMH; solid squares IMH.

Neutron detection in HALO is imperfect, as neutrons generated in the lead may escape without passing through a ^{3}He counter. As a result, 1n and 2n events may go undetected, and 2n events may be misidentified as 1n events. These effects are quantified by the efficiency matrix,

$$M = \begin{pmatrix} \text{1n measured as 1n} & \text{2n measured as 1n} \\ \text{1n measured as 2n} & \text{2n measured as 2n} \end{pmatrix}, \tag{4.2}$$

where the matrix entries are fractional rates. With this matrix, the detection of neutrons in HALO can be modeled as a linear transformation on the truth data:

$$\begin{pmatrix} N_{\text{1n observed}} \\ N_{\text{2n observed}} \end{pmatrix} = M \begin{pmatrix} N_{\text{1n true}} \\ N_{\text{2n true}} \end{pmatrix}. \tag{4.3}$$

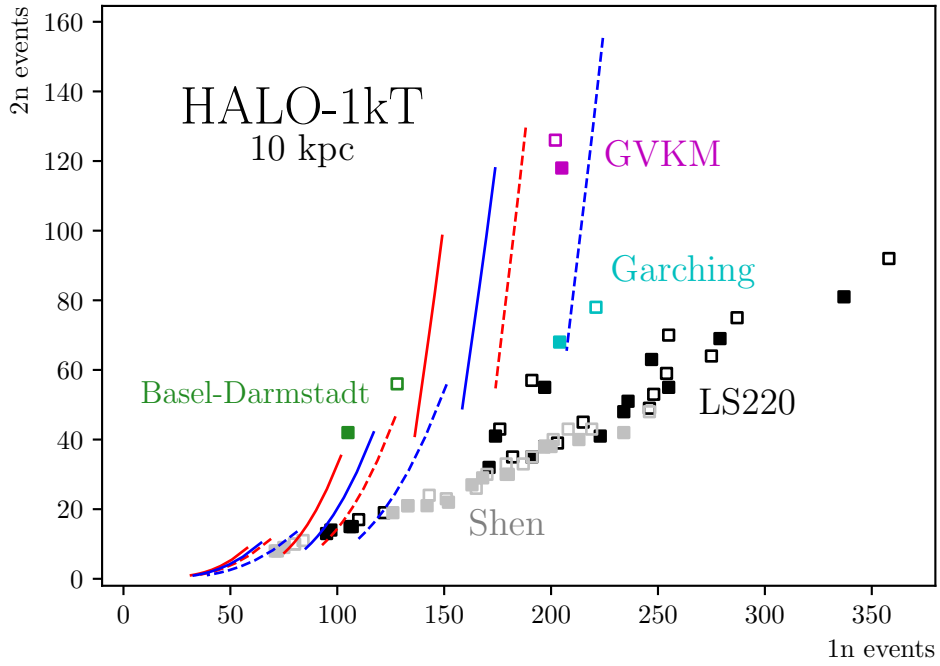

Figure 4.4: Same as Figure 4.3, rescaled for HALO-1kT by 1/0.079.

The goal is to determine the entries of the efficiency matrix, so that we can estimate the observed number of neutrons for a given event. This is done with Geant4.

To determine HALO's detection efficiencies, I used the HALO Collaboration's full simulation of the detector built in Geant4 (revision 199, last changed Aug. 27, 2016). Given neutron positions and momenta, Geant4 simulates the movement and interactions of the particles, and records any charge depositions in the neutron counters. As detection of neutrons in HALO is approximately independent of initial neutron direction [25], I simulated 10,000 randomly-positioned isotropic 1n and 2n events for each 0.5 MeV step in the range 0.5 - 10 MeV. A representative distribution of charge depositions in the ^{3}He counters is shown in Figure 4.5.

When neutrons are captured by ^{3}He, a 573 keV proton and a 191 keV triton are produced. The 764 keV peak in Figure 4.5 corresponds to the case where both of these particles deposit all of their energy in the neutron counter. When the neutron is captured near the edge of the counter, one or both of the particles might escape before depositing all of their energy. This

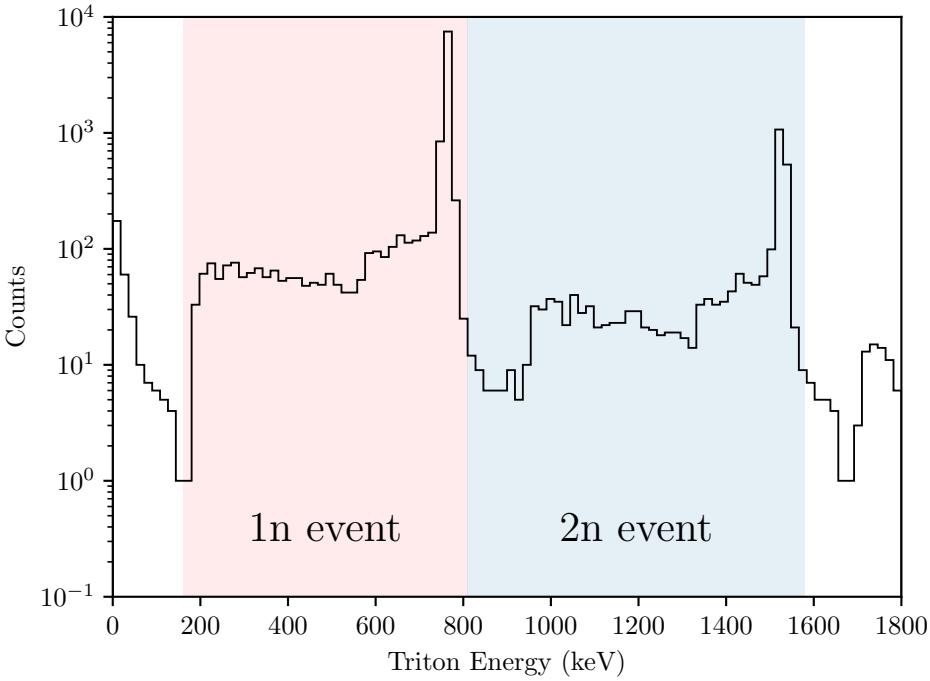

Figure 4.5: Distribution of charge depositions in HALO ^{3}He counters due to ten thousand 250 MeV 1n and 2n events. Energies characteristic of a 1n event are highlighted in red, while energies characteristic of 2n events are highlighted in blue.

results in the two-tiered structure to the left of the 764 keV peak. The distribution in blue, to the right of the 764 keV peak, is the result of both neutrons in a 2n event being captured in the same counter. Thus, the energy deposition in a single ^{3}He counter can be used to discriminate between 1n and 2n detections. Of course, simultaneous charge depositions in two different counters also indicate a 2n event.

The quantities and locations of charge depositions were used to tag 1n and 2n events, and the detected numbers were compared to the truth values. The HALO detection efficiencies are displayed as a function of energy in Figure 4.6. Aside from the increase in 2n detections past 8 MeV, the efficiencies are approximately independent of energy. As neutrons from neutrino interactions with lead are typically expected to have energies less than 6 MeV [15], the efficiencies for neutrons less than 6 MeV are averaged and used in the efficiency matrix:

$$M = \begin{pmatrix} 0.266 & 0.362 \\ 0 & 0.086 \end{pmatrix}. \tag{4.4}$$

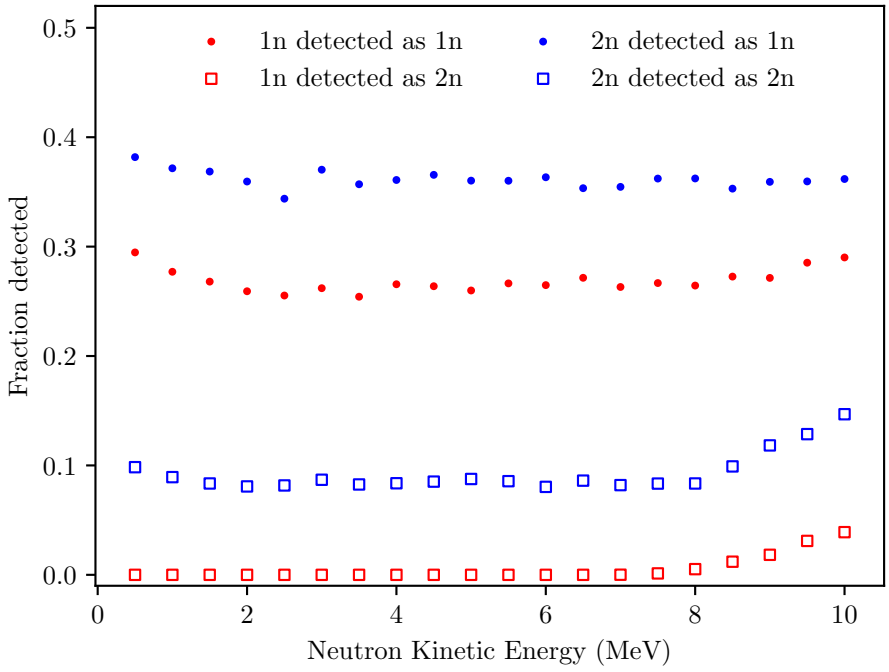

Figure 4.6: HALO detection efficiencies as a function of neutron energy.

These values are further refined using experimental data from the HALO calibration performed by Colin Bruulsema. Assuming that the probability of each neutron detection in a 2n event is independent, it is expected that

$$M = \begin{pmatrix} \epsilon & 2\epsilon(1-\epsilon) \\ 0 & \epsilon^2 \end{pmatrix}, \tag{4.5}$$

where ϵ is the probability of detecting a single neutron. Using $\epsilon = 0.266$ as determined in the HALO Geant4 simulation, we calculate

$$M = \begin{pmatrix} 0.266 & 0.390 \\ 0 & 0.071 \end{pmatrix}. \tag{4.6}$$

It is seen that, when compared to the Geant4 simulation (Equation 4.4), calculating the efficiencies using Equation 4.5 overestimates the number of 2n events detected as 1n events and underestimates the number of 2n events detected as 2n events.

The 1n as 1n detection efficiency, ϵ, was measured by Colin Bruulsema by placing calibrated neutron sources in the HALO detector [14]. His analysis yielded $\epsilon = 0.283 \pm 0.002$ for

a uniform distribution of neutrons, created in the lead volume with energies according to the distribution for supernova neutrinos interacting with lead. This result, which is greater than the efficiency from the Geant4 simulation, is used to calculate the efficiencies used in the rest of this thesis. These values are further adjusted according to the discrepancies between Equations 4.4 and 4.6. Element M_{ij} is multiplied by the ratio

$$\frac{M_{ij} \text{ from Geant4}}{M_{ij} \text{ as calculated using } \epsilon_{\text{ Geant4}}}. \tag{4.7}$$

Thus the efficiencies used hereafter are

$$M_{\text{HALO}} = \begin{pmatrix} 0.283 & 0.376 \\ 0 & 0.097 \end{pmatrix}. \tag{4.8}$$

A similar efficiency matrix is constructed for HALO-1kT. As mentioned in Section 4.1, the truth numbers for HALO-1kT are simply calculated from the HALO event numbers via scaling by the mass ratio (1/0.079). Recent Monte Carlo simulations of the proposed HALO-1kT design indicate that HALO-1kT will have a single-neutron detection efficiency of about $\epsilon = 0.53$ [17]. For this thesis, a HALO-1kT efficiency matrix is calculated for this ϵ using Equation 4.5:

$$M_{\text{HALO-1kT}} = \begin{pmatrix} 0.53 & 0.498 \\ 0 & 0.281 \end{pmatrix}. \tag{4.9}$$

5

Data Unfolding Studies

Of the 1n and 2n events that occur in HALO, only a fraction are detected and some of those are misidentified. As the relative number of 1n and 2n events are sensitive to the supernova neutrino spectrum, it is important to develop a method for reconstructing true 1n and 2n event numbers from detected events. This process, called "unfolding," is the focus of this chapter. Two methods are examined: the first uses the inverted efficiency matrix, which produces large uncertainties and unphysical results. The second is a Bayesian algorithm, which uses supernova neutrino flux models and astrophysical data to improve on these problems.

5.1 Matrix Inversion Method

The simplest unfolding can be performed by inverting Equation 4.3:

$$\begin{pmatrix} N_{\text{1n true}} \\ N_{\text{2n true}} \end{pmatrix} = M^{-1} \begin{pmatrix} N_{\text{1n observed}} \\ N_{\text{2n observed}} \end{pmatrix}. \tag{5.1}$$

In principle, this method should yield perfect results; however, variations of the detection efficiency across the detector and Poisson error lead to imperfect unfolding. To understand the precision and limitations of this method, Monte Carlo simulations of the detection and unfolding process were compared to truth values.

Ten thousand supernovae were simulated, each with a number of 1n and 2n truth events sampled from a 2D Poisson distribution centered on a chosen truth value. The number of detected events is calculated for each one of these 1n-2n pairs with a toy Monte Carlo, using the efficiencies from the efficiency matrix. These "detected" data points are then unfolded

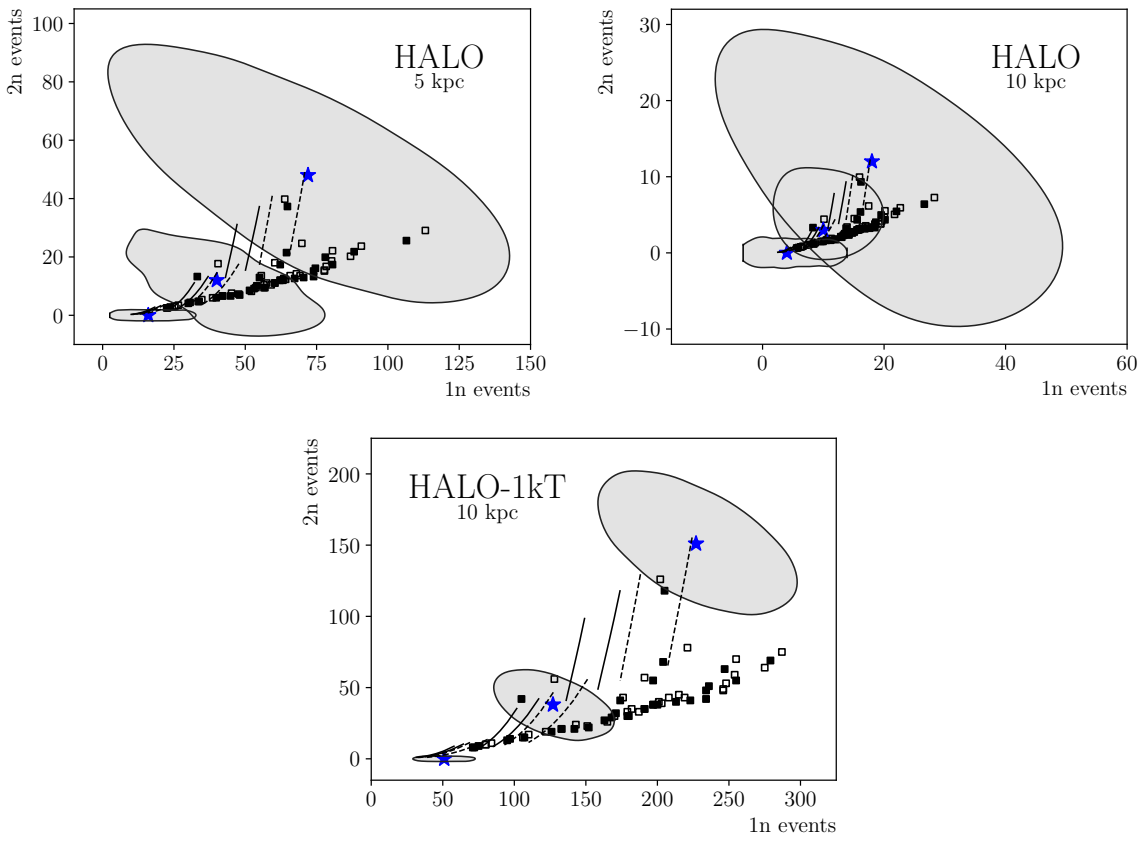

Figure 5.1: Matrix inversion unfolding for HALO at 5 and 10 kpc, and HALO-1kT at 10 kpc. The stars represent sample truth values. For HALO at 5 kpc, these are (1n,2n) = {(72, 48), (40, 12), (16, 0)}. They are rescaled appropriately for HALO at 10 kpc and for HALO-1kT. The gray contours contain 90% of the respective unfolded values. The expected 1n, 2n values from Figure 4.3 are overlaid in black for reference.

using Equation 5.1. The results of this unfolding are visualized by drawing a contour around 90% of the unfolded data points in the 1n-2n event space.

The results of this study for HALO at 5 and 10 kpc, and HALO-1kT at 10 kpc are shown in Figure 5.1. The blue stars represent three different truth values, chosen from the distribution of supernova models, which are plotted in black. These are the same points from Figure 4.3. The gray contours represent 90% of the unfolded points.

It can be seen from the gray contours in Figure 5.1 that the matrix unfolding is unstable. The Poisson noise in the detection leads to a wide range of unfolded values. This leads to in large uncertainties and unphysical results. In addition, there are unfolding results that lie

well outside the distribution of supernova neutrino models plotted in Figure 4.3, and there is significant overlap between the HALO unfolding contours of different supernova models for supernovae at 10 kpc. In the next section, Bayesian statistics are used to alleviate these problems.

5.2 Bayesian Method

In order to eliminate unphysical results and reduce uncertainty, Bayesian statistics are used. Let the true number of 1n and 2n events be labeled as the "cause" C_{ij} and the observed number be labeled as the "effect" E_{ij}, where i and j are the number of 1n and 2n events, respectively. Then the reconstructed probability distribution $\hat{n}(C_{ij})$ can be calculated via Bayes' Theorem:

$$\hat{n}(C_{ij}) = \sum_{m,n} n(E_{mn}) P(C_{ij}|E_{mn}) = \sum_{m,n} n(E_{mn}) \frac{P(E_{mn}|C_{ij}) P(C_{ij})}{P(E_{mn})}, \tag{5.2}$$

where $n(E_{ij})$ is the observed distribution. Note that in the case of a real supernova detection in HALO, $n(E_{ij})$ will be a delta function, and no sum over observed event numbers will be required.

Equation 5.2 can be recast as

$$\hat{n}(C_{ij}) = \sum_{m,n} n(E_{mn}) R_{ij,mn} \ , \tag{5.3}$$

where $R_{ij,mn}$ is the so-called "response matrix" [26]. The response matrix depends on a prior distribution of causes, $P(C_{ij})$, and the probabilities $P(E_{mn}|C_{ij})$ and $P(E_{mn})$, which can be determined via a Monte Carlo simulation using the efficiency matrix.

Estimation of the response matrix and the subsequent Bayesian unfolding is performed with RooUnfold [27], a data unfolding library in Root[1]. The prior distribution of true 1n and

[1]RooUnfold's algorithm iterates the unfolding to achieve better results, however this requires an ensemble of detections. In the event of a supernova, HALO will only make one detection (i.e. one 1n, 2n pair will be recorded). Thus when using the RooUnfold algorithm, the number of iterations must be set to one.

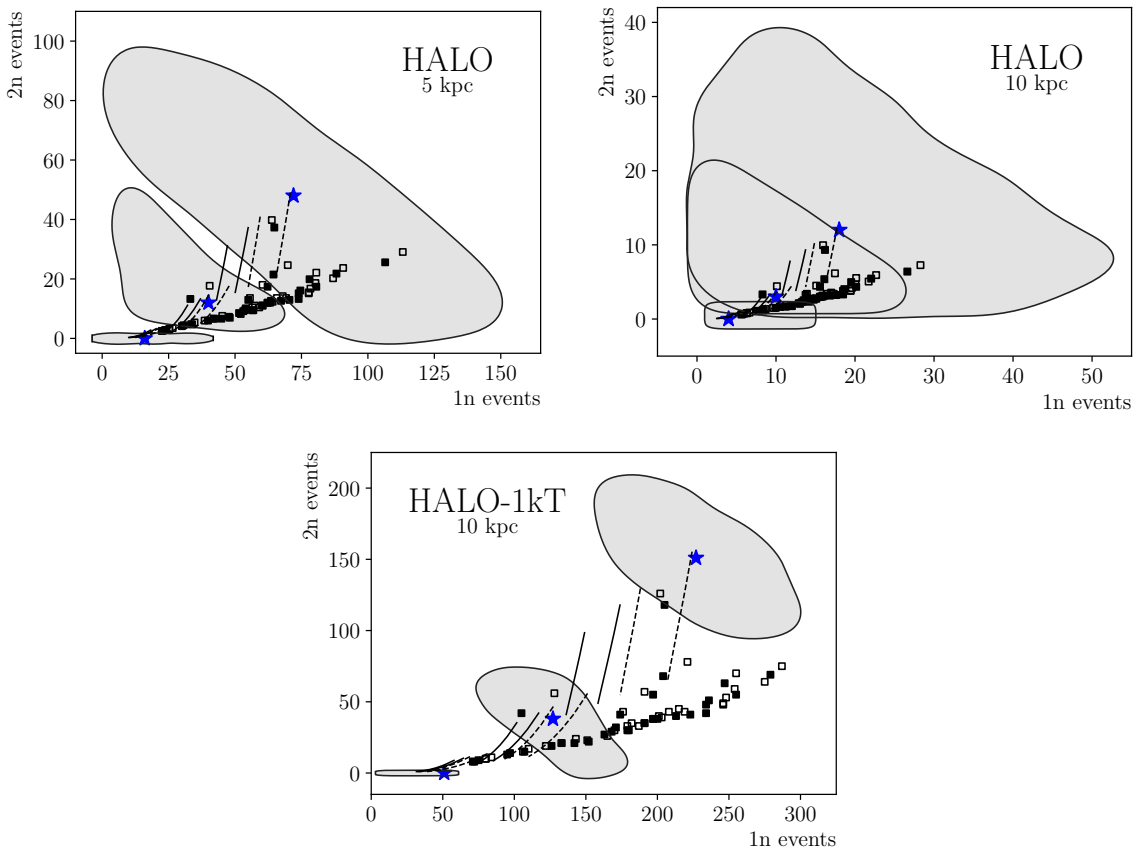

Figure 5.2: Unfolding with the positive plane prior (prior 1). Gray contours contain 90% of unfolded points. Blue stars represent truth points; black points and curves represent expected 1n, 2n events for various supernova models.

2n events in HALO, $P(C_{ij})$, is constructed with reference to the expected event numbers in Figure 4.3. The "observed prior," $P(E_{mn})$, is created by applying the efficiency matrix to the distribution in the prior.

Three different priors with varying levels of assumptions are considered. The most conservative prior is a uniformly populated, positive 1n-2n plane. This prior merely restricts the unfolding to event numbers greater than or equal to zero, eliminating unphysical results, but makes no assumptions about neutrino flux models or supernova distances. The results of this unfolding are shown in Figure 5.2. These contours resemble the contours from the matrix-inversion unfolding, without the unphysical predictions.

The second prior ("distance unknown"), seen on the left in Figure 5.3, assumes that the

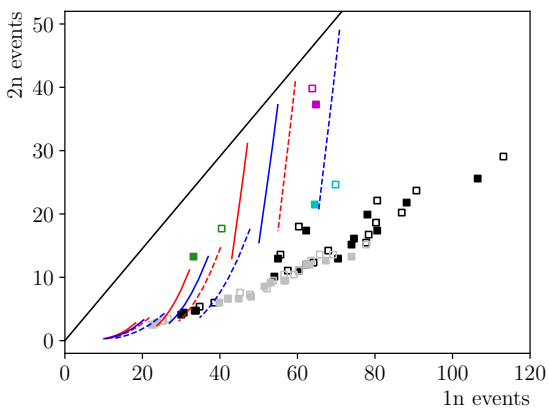

(a) Prior 2: Distance Unknown

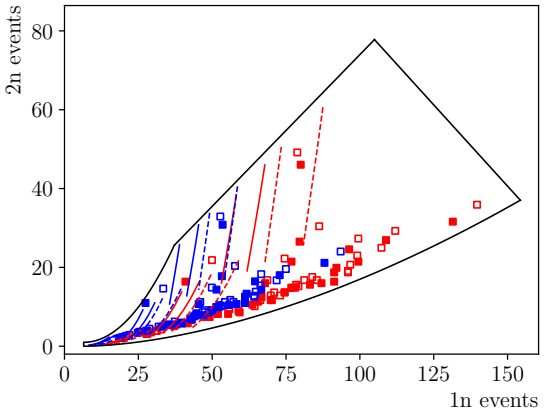

(b) Prior 3: Distance Known

Figure 5.3: Two versions of the prior, $P(C_{ij})$. Left: a maximum ratio $2n/1n$ is imposed for the distance unknown prior, which consists of a uniform distribution in the positive 1n-2n plane below this cut. Right: expected 1n, 2n values from Figure 4.3 are plotted twice, once for 4.5 kpc (red) and once for 5.5 kpc (blue). An envelope containing these points is used for the distance known prior, which consists of a uniform distribution inside the envelope.

models in Figure 4.3 represent an accurate range of possible supernova neutrino fluxes, but makes no assumption about the supernova distance. Since 1n and 2n values scale with distance by the same factor, it is possible to impose a maximum ratio $2n/1n$ for expected events in HALO (the black line in Figure 5.3a). The second prior features a uniform distribution below this line. The results of this unfolding, seen in Figure 5.4, show significant improvements. Just as the positive plane prior prevents predictions of unphysical event numbers, the distance-unknown prior prevents predictions of $2n/1n$ ratios far above those predicted by the range of theoretical models. However, this has potential to introduce bias if the models on which the priors are based are inaccurate. Proposals for how to alleviate this problem are discussed in Section 5.3.

The third prior ("distance known"), seen on the right in Figure 5.3, assumes that the models in Figure 4.3 are accurate and that the distance to the supernova is known within 10%. Figure 5.3b shows the models from Figure 4.3 plotted twice: once for 4.5 kpc (in red) and once for 5.5 kpc (in blue). An envelope is drawn around these two sets, imposing further constraints on the event space. The unfolding is performed using a prior consisting of a uniform distribution inside this envelope. The results are displayed in Figure 5.5. The addition

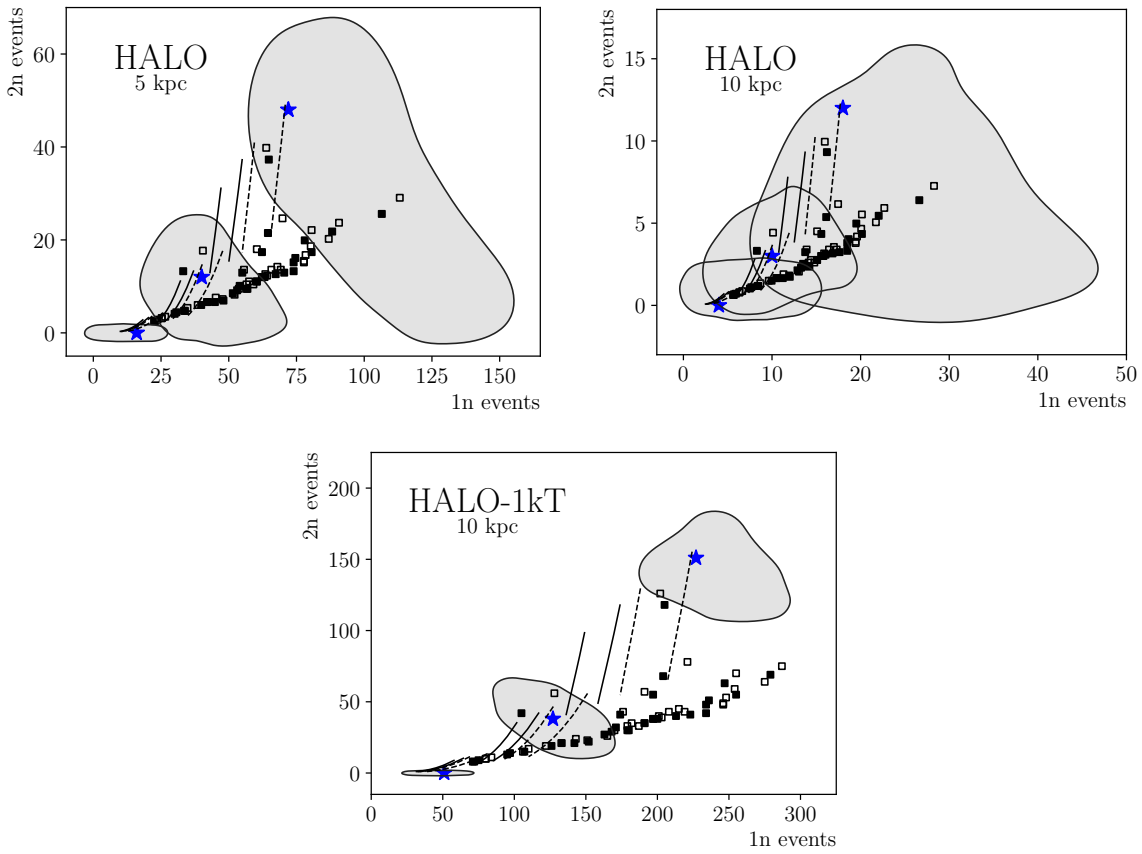

Figure 5.4: Unfolding with the distance unknown prior (prior 2). Gray contours contain 90% of unfolded points. Blue stars represent truth points; black points and curves represent expected 1n, 2n events for various supernova models.

of information about the supernova distance further improves the HALO analysis and reduces uncertainty in the unfolding. Similar priors can be made for any given distance uncertainty. Notice that at 10 kpc, there is still significant overlap for HALO but not for HALO-1kT. The effect of supernova distance on HALO's discriminatory power will be evaluated in Chapter 6.

5.3 Further improvements

This chapter demonstrated how data unfolding for HALO can be improved with Bayesian statistics. This method significantly reduces the size of the unfolding contours, however this comes with the risk of biasing the results. The accuracy of the Bayesian unfolding depends on the selected prior, which in turn relies on our knowledge of supernova neutrino fluxes.

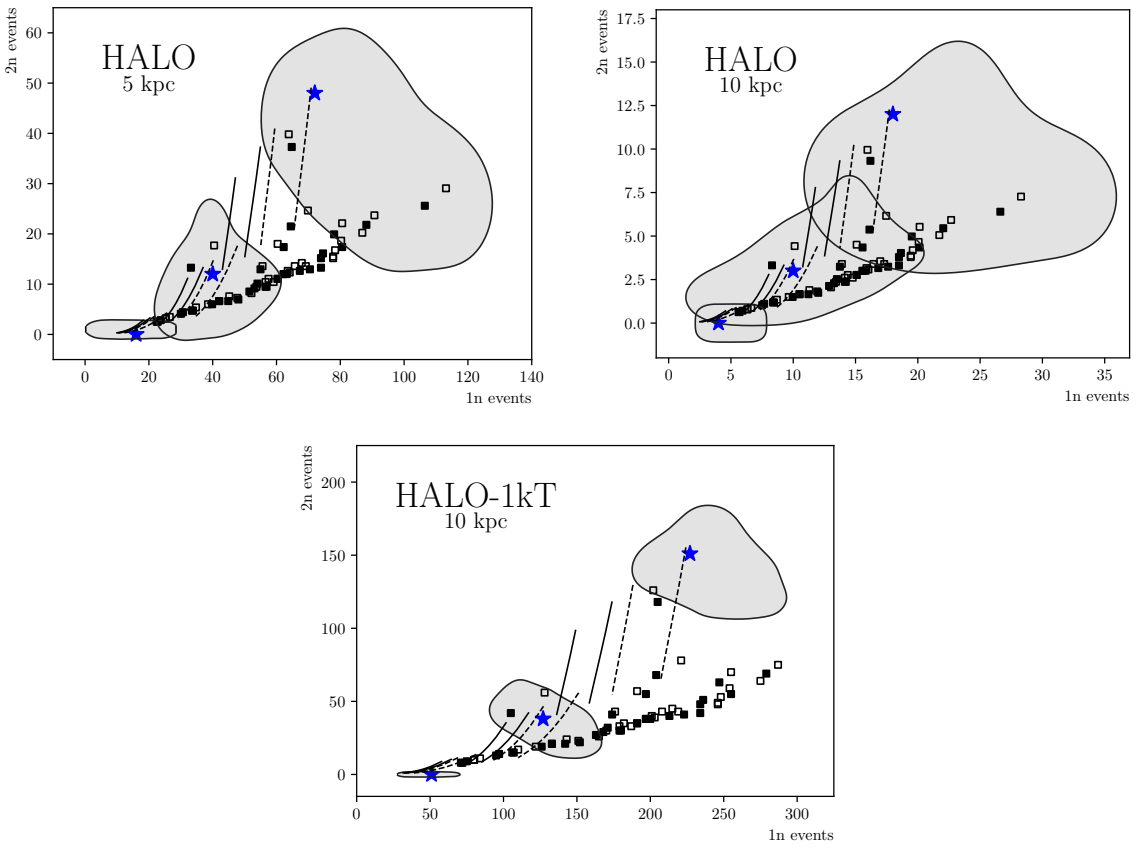

Figure 5.5: Unfolding with the distance known prior (prior 3). Gray contours contain 90% of unfolded points. Blue stars represent truth points; black points and curves represent expected 1n, 2n events for various supernova models.

The priors used above feature a uniform distribution in a given area of the 1n-2n plane, surrounded by a sharp cutoff to zero. If the truth event lies outside the cutoff, then the unfolding will be inaccurate, as the prior assumes zero probability for these regions. This problem can be avoided altogether by using the positive plane prior, but smearing the more restrictive priors may yield better results. A "smeared" prior would resemble the original prior, but with a more gradual decrease to zero on the edges. This may reduce the bias without such a large increase in contour size.

It may also be worthwhile to investigate other unfolding methods. In addition to the matrix inversion and Bayesian methods explained here, I also attempted unfolding with a neural network. I used a dense, feed-forward neural network, which was trained on large

sets of truth and observed values. This method yielded very similar results to the Bayesian unfolding, but as neural networks are more complex, opaque, and difficult to train, the method was abandoned.

6

Detector Sensitivity Versus Supernova Distance

The sensitivities of HALO and HALO-1kT decrease with supernova distance. As the number of 1n and 2n events decrease, the relative size and overlap of the contours increase. This can be seen by comparing the 5 and 10 kpc unfoldings for HALO in Figures 5.1, 5.4, and 5.5. The Bayesian priors present a natural way to quantify this decrease in sensitivity. To do this, I calculate the percentage of reasonable models (i.e. percentage of the prior) that is excluded by the contour:

$$\text{fraction of models excluded} = 1 - \frac{\text{area of contour}}{\text{area of prior}}. \tag{6.1}$$

A figure of merit is created for HALO by plotting the fraction of models excluded versus the supernova distance (Figure 6.1). The distance known prior is used, assuming a distance uncertainty of 10%. Notice that the fraction of models excluded is approximately 0.5 at 5 kpc and is zero at 10 kpc. This suggests that the sensitivity of HALO is roughly limited to 5 kpc, with weak sensitivity in the range 5-10 kpc. Note that the most likely distance to a galactic supernova is approximately 10 kpc [10].

The figure of merit for HALO can be extended to different distance uncertainties. Figure 6.2 shows the fractional model exclusions as a function of supernova distance and distance uncertainty. It is seen that distance uncertainties $\leq 10\%$ yield much better distance sensitivity, however, somewhat surprisingly, the distance sensitivity is only weakly dependent on the distance uncertainty for uncertainties $> 10\%$.

HALO's limited distance sensitivity is highly restrictive, as it indicates that HALO will

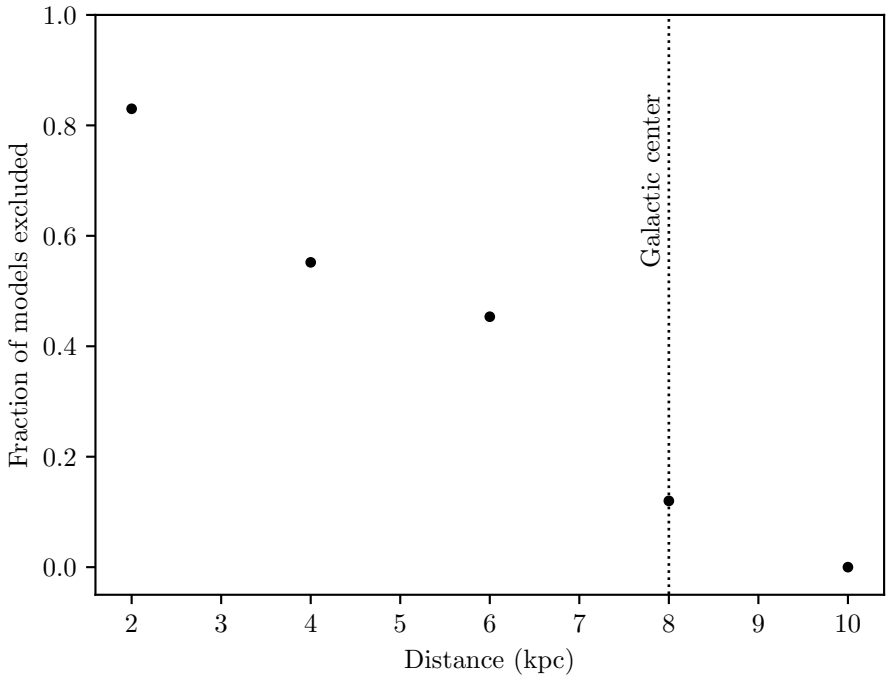

Figure 6.1: Figure of merit for HALO, using the distance known prior, assuming supernova distance is known within 10%. The fraction of supernova models excluded is plotted on the y-axis. This fraction is approximately 0.5 at 5 kpc and 0 at 10 kpc. The dotted vertical line indicates the distance to the galactic center.

likely have little sensitivity to the next galactic supernova, and will have difficulty distinguishing between the different supernova neutrino flux models in Figure 4.3. This limitation is a strong motivator for HALO-1kT.

HALO-1kT fares much better for supernovae at 10 kpc (c.f. Figures 5.1, 5.4, and 5.5), indicating that HALO-1kT will have a much greater distance range. The figure of merit for HALO-1kT, using the distance known prior and assuming distance uncertainty of 10%, is shown in Figure 6.3. This figure of merit assumes the HALO-1kT efficiencies in Equation 4.9. The fraction of models excluded is approximately 0.5 at 25 kpc and 0 at 50 kpc. This surpasses the HALO range by a factor of 5, and encompasses the entire Milky Way Galaxy, which has a radius of around 25 kpc. In addition, HALO-1kT has weak sensitivity approximately reaching the Large Magellanic Cloud, which is aout 50 kpc from Earth [28].

Similarly to HALO, the HALO-1kT figure of merit can be generalized to other distance

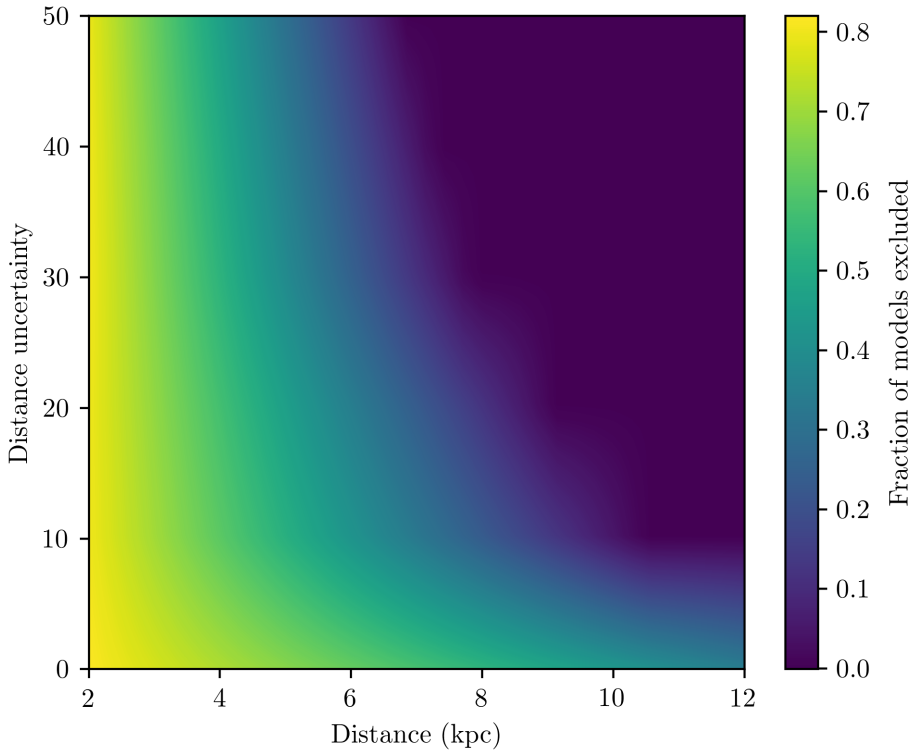

Figure 6.2: Figure of merit for HALO, using the distance known prior. The fraction of supernova models excluded is plotted on the z-axis, as a function of supernova distance (x-axis) and distance uncertainty (y-axis).

uncertainties. In addition, as the final design of HALO-1kT is not yet finalized and the neutron detection efficiencies are not yet determined, it is useful to extend the HALO-1kT figure of merit to include dependence on the 1n detection efficiency, ϵ. This is shown in Figure 6.4.

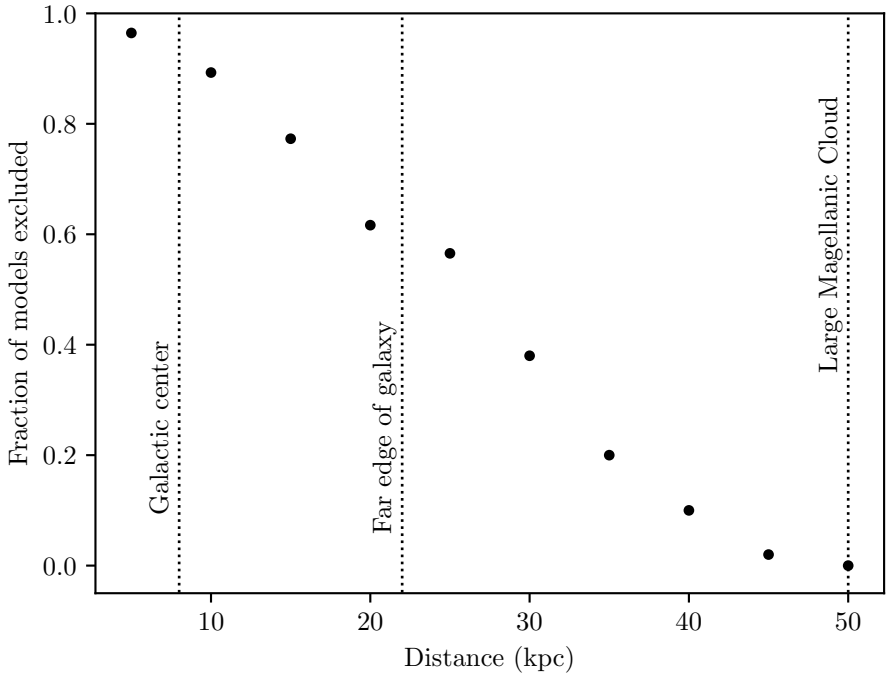

Figure 6.3: Figure of merit for HALO-1kT, using the distance known prior, assuming supernova distance is known within 10%. The HALO-1kT detection efficiences are given by Equation 4.9. The fraction of supernova models excluded is plotted on the y-axis. This fraction is approximately 0.5 at 25 kpc and 0 at 50 kpc, greatly extending the sensitivity range of HALO. Dotted vertical lines indicate reference distances.

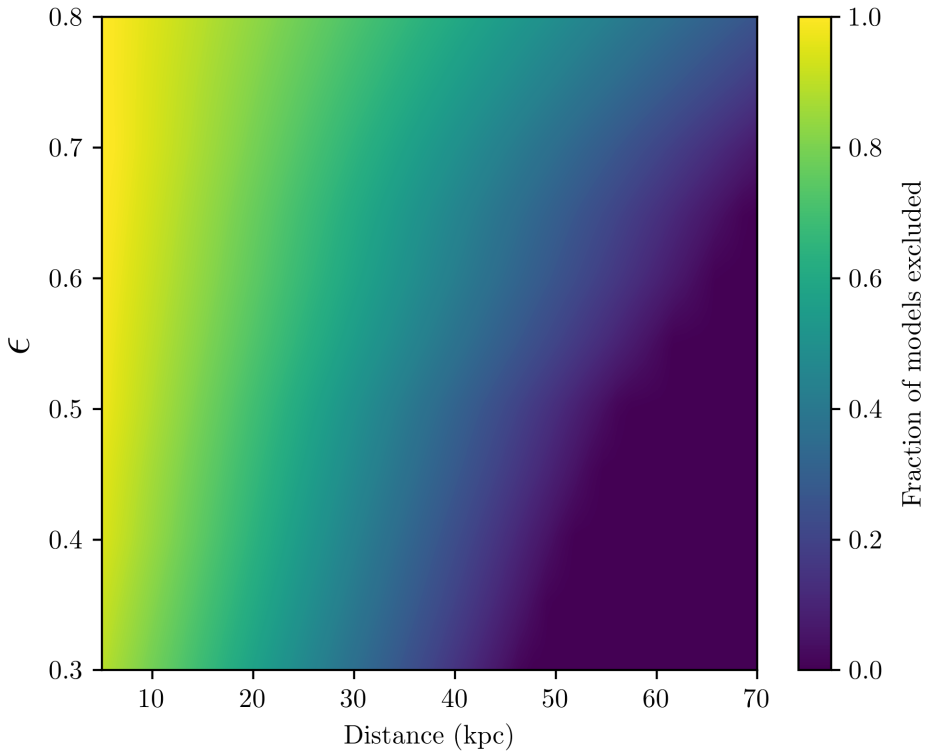

Figure 6.4: Figure of merit for HALO-1kT, using the distance known prior and assuming the distance uncertainty is 10%. The fraction of supernova models excluded is plotted on the z-axis, as a function of supernova distance (x-axis) and 1n detection efficiency, ϵ (y-axis).

7

Conclusion

Core-collapse supernovae produce prodigious amounts of neutrinos in the tens of MeV range. Detecting these neutrinos are of high scientific interest. Neutrinos carry information about supernova dynamics out of the dense cores of dying stars. Supernova neutrinos also provide an opportunity to observe collective neutrino interactions and serve as an advanced warning of an impending optical signal. The Helium and Lead Observatory (HALO) hopes to detect these supernova neutrino bursts via charged- and neutral-current interactions with lead nuclei.

The expected signal in HALO for a galactic core-collapse supernova was studied in Chapter 4, using a full detector simulation in Geant4, simpler toy Monte Carlo simulations, and the SNOwGLoBES neutrino event rate calculator. In the case of a galactic supernova within 10 kpc, we expect tens of 1n and 2n events in the lead matrix, about a third of which will be detected in HALO's ^{3}He counters. In order to extract information about the neutrino spectra, we must unfold the detected event numbers to reconstruct truth numbers.

In Chapter 5, two different data unfolding techniques were examined. The first method, unfolding via inverting the matrix of HALO detection efficiencies, is unstable, with large uncertainties and unphysical predictions. A Bayesian algorithm improves the unfolding. The priors for the Bayesian algorithm are constructed with reference to the expected range of neutrino flux parameters and the precision with which the supernova distance is determined. This method balances reducing uncertainty and increasing the risk of bias, depending on how conservative the selected prior is.

The Bayesian priors present a natural method for quantifying the sensitivity of HALO as a function of distance. In Chapter 6, HALO sensitivity is determined by calculating the

percentage of the prior that is excluded by the final unfolding results. The percent of the prior excluded decreases as a function of distance. These studies reveal that HALO is only weakly sensitive to supernovae past 5 kpc, and has no sensitivity to supernovae farther than 10 kpc. This is problematic, as the most likely distance to a supernova is approximately 10 kpc, and much of our galaxy is farther than 10 kpc from Earth.

These results motivate the development of HALO-1kT, the proposed 1 kiloton upgrade to HALO at Gran Sasso National Laboratory (LNGS) in Italy. Due to the larger mass, HALO-1kT expects event numbers greater than ten times that of HALO, and simulations of the proposed detector design indicate that the upgrade's detection efficiencies will be almost twice that of HALO. These improvements greatly reduce the uncertainties in the data unfolding and extend HALO-1kT's sensitivity by a factor of 5. This distance covers our entire galaxy and approximately reaches the Large Magellanic Cloud.

In order to further improve the unfolding process, it is vital that the effect of collective neutrino oscillations are incorporated into the SNOwGLoBES event rates. Without considering collective effects, we cannot be sure of the correct limits to place on the Bayesian priors. In addition, the sharp cutoffs on the priors could be smoothed. This will likely reduce bias in the case that there are viable neutrino flux models not included in our priors.

Regardless, HALO is waiting patiently, along with a large network of neutrino detectors across the globe, ready to record the neutrino burst of the next core-collapse supernova in our galaxy. The scientific yield of such an event will be substantial, and hopefully SNEWS will allow astronomers to observe the explosion as well, opening a multi-messenger window on one of the most spectacular events in the universe.

Appendix: Other event numbers in HALO

Event numbers for Garching, GVKM, Basel-Darmstadt, LS220, and Shen fluxes. All values are events in HALO for a supernova at 5 kpc. Values can be rescaled to different supernova distances (by $1/r^2$) and for HALO-1kT (by the mass ratio 1/0.079).

	NMH		IMH		
Flux	1n	2n	1n	2n	Reference
Garching	70	25	64	21	[21]
GVKM	64	40	65	39	[22]
Basel-Darmstadt	40	18	33	13	[23]
LS220-ss11.2	106	15	95	13	[24]
LS220-ss11.2c	122	19	107	15	
LS220-ss11.2co	110	17	97	14	
LS220-ss25.0	287	75	279	69	
LS220-ss25.0o	191	57	197	55	
LS220-ss25.0c	358	92	337	81	
LS220-ss25.0co	255	70	247	63	
LS220-ss27.0	203	39	191	35	
LS220-ss27.0o	182	35	171	32	
LS220-ss27.0c	246	49	223	41	
LS220-ss27.0co	215	45	197	38	
LS220-ss40.0	248	53	234	48	
LS220-ss40.0o	176	43	174	41	
LS220-ss40.0c	275	64	255	55	
LS220-ss40.0co	254	59	236	51	
Shen-s11.2	80	10	72	8	
Shen-s11.2c	84	11	75	9	
Shen-s11.2co	80	10	71	8	
Shen-s25.0	219	43	213	40	
Shen-s25.0o	201	40	197	38	
Shen-s25.0c	246	48	234	42	
Shen-s25.0co	208	43	200	38	
Shen-s27.0	151	23	142	21	
Shen-s27.0o	133	21	126	19	
Shen-s27.0c	165	26	152	22	
Shen-s27.0co	143	24	133	21	
Shen-s40.0	187	33	180	30	
Shen-s40.0o	170	30	163	27	
Shen-s40.0c	191	35	179	30	
Shen-s40.0co	179	33	168	29	

References

[1] *https://commons.wikimedia.org/wiki/File:Elementary_particle_interactions_in_the_Standard_Model.png*

[2] A. Palazzo, *Phenomenology of light sterile neutrinos: a brief review*, Modern Physics Letters A **28** (2013) (07)

[3] G. Fantini, A. Gallo Rosso, V. Zema and F. Vissani, *Introduction to the Formalism of Neutrino Oscillations*, in A. Ereditato (ed.), *The State of the Art of Neutrino Physics* (World Scientific Publishing, Toh Tuck Link, Singapore, 2018), pp. 37–119

[4] B. Ryden, *Introduction to Cosmology*, 2nd ed. (Cambridge University Press, 2016)

[5] M. Wascko, *T2K Status, Results, and Plans*, in *Proceedings of the 28th International Conference on Neutrino Physics and Astrophysics* (2018)

[6] M. Sanchez, *NOvA Results and Prospects*, in *Proceedings of the 28th International Conference on Neutrino Physics and Astrophysics* (2018)

[7] P. Coloma and S. Pascoli, *Theory and Phenomenology of Mass Ordering and CP Violation*, in A. Ereditato (ed.), *The State of the Art of Neutrino Physics* (World Scientific Publishing, Toh Tuck Link, Singapore, 2018), pp. 497–542

[8] B. Ryden and B. Peterson, *Foundations of Astrophysics* (Addison-Wesley, 2010)

[9] A. Burrows, *Supernova explosions in the Universe*, Nature **403** (2000) (6771), pp. 727–733

[10] K. Scholberg, *Neutrinos from Supernovae and Other Astrophysical Sources*, in A. Ereditato (ed.), *The State of the Art of Neutrino Physics* (World Scientific Publishing, Toh Tuck Link, Singapore, 2018), pp. 299–324

[11] A. Mirizzi, I. Tamborra, H.-T. Janka, N. Saviano, K. Scholberg, R. Bollig, L. Hudepohl and S. Chakraborty, *Supernova Neutrinos: Production, Oscillations and Detection* (2015)

[12] F. Vissani, *Comparative analysis of SN1987A antineutrino fluence*, Journal of Physics G Nuclear Physics **42** (2015) (1), 013001

[13] K. Scholberg, *The SuperNova Early Warning System* (2008)

[14] C. Bruulsema, *Calibration and Commissioning of the Helium And Lead Observatory*, Master's thesis, Laurentian University (2017)

[15] E. Kolbe and K. Langanke, *Role of* $\nu -$ induced *reactions on lead and iron in neutrino detectors*, Phys. Rev. C **63** (2001)

[16] J. Engel, G. C. McLaughlin and C. Volpe, *What Can Be Learned with a Lead-Based Supernova-Neutrino Detector?* (2002)

[17] B. Pointon, *HALO-1kT - Helium and Lead Observatory for Supernova Neutrinos with High Sensitivity to ν_e*, in *Proceedings of the 28th International Conference on Neutrino Physics and Astrophysics* (2018)

[18] M. T. Keil, G. G. Raffelt and H.-T. Janka, *Monte Carlo Study of Supernova Neutrino Spectra Formation* (2002)

[19] D. Väänänen and C. Volpe, *The neutrino signal at HALO: learning about the primary supernova neutrino fluxes and neutrino properties*, Journal of Cosmology and Astroparticle Physics **2011** (2011)

[20] A. Beck, F. Beroz, R. Carr, H. Duan, A. Friedland, N. Kaiser, J. Kneller, A. Moss, D. Reitzner, K. Scholberg, D. Webber and R. Wendell, *SNOwGLoBES: SuperNova Observatories with GLoBES: DRAFT* (2013)

[21] L. Hüdepohl, B. Müller, H.-T. Janka, A. Marek and G. G. Raffelt, *Neutrino Signal of Electron-Capture Supernovae from Core Collapse to Cooling*, Phys. Rev. Lett. **104** (2010)

[22] J. Gava, J. Kneller, C. Volpe and G. C. McLaughlin, *Dynamical Collective Calculation of Supernova Neutrino Signals*, Phys. Rev. Lett. **103** (2009)

[23] A. Bandyopadhyay, P. Bhattacharjee, S. Chakraborty, K. Kar and S. Saha, *Detecting supernova neutrinos with iron and lead detectors*, Phys. Rev. D **95** (2017)

[24] L. Hüdepohl, *Neutrinos from the Formation, Cooling and Black Hole Collapse of Neutron Stars*, Ph.D. thesis, Technische Universität München (2014)

[25] C. Esposito and K. Scholberg, *Efficiency and Sensitivity Updates for the HALO Simulation*, Tech. rep., Duke University (2013)

[26] G. D'Agostini, *A multidimensional unfolding method based on Bayes' theorem*, Nuclear Instruments and Methods in Physics Research Section A: Accelerators, Spectrometers, Detectors and Associated Equipment **362** (1995) (2-3), pp. 487–498

[27] T. Adye, *Unfolding algorithms and tests using RooUnfold*, in *Proceedings of PHYSTAT 2011* (CERN, 2011), pp. 313–318

[28] G. Pietrzyński, D. Graczyk, W. Gieren, I. B. Thompson, B. Pilecki, A. Udalski, I. Soszyński, S. Kozłowski, P. Konorski, K. Suchomska, G. Bono, P. G. P. Moroni, S. Villanova, N. Nardetto, F. Bresolin, R. P. Kudritzki, J. Storm, A. Gallenne, R. Smolec, D. Minniti, M. Kubiak, M. K. Szymański, R. Poleski, Ł. Wyrzykowski, K. Ulaczyk, P. Pietrukowicz, M. Górski and P. Karczmarek, *An eclipsing-binary distance to the Large Magellanic Cloud accurate to two per cent*, **495** (2013) (7439), pp. 76–79